Review article **Open Access**

Martin Ams*, Peter Dekker, Simon Gross and Michael J. Withford

Fabricating waveguide Bragg gratings (WBGs) in bulk materials using ultrashort laser pulses

DOI 10.1515/nanoph-2016-0119
Received May 24, 2016; revised August 17, 2016; accepted September 14, 2016

Abstract: Optical waveguide Bragg gratings (WBGs) can be created in transparent materials using femtosecond laser pulses. The technique is conducted without the need for lithography, ion-beam fabrication methods, or clean room facilities. This paper reviews the field of ultrafast laser-inscribed WBGs since its inception, with a particular focus on fabrication techniques, WBG characteristics, WBG types, and WBG applications.

Keywords: ultrafast; laser; waveguide; Bragg; grating.

1 Introduction

Focussed ultrashort laser pulses can modify the refractive index inside materials such as glass, crystal, and polymer [1–3]. This phenomenon led to a new field in photonics, whereby optical waveguide devices can be directly written into the volume of bulk materials simply by moving the sample through the laser focus, as shown in Figure 1. Not only can this direct-write technique be carried out rapidly, but also photonic devices can be written at arbitrary depths inside a material and in a 3D fashion. The technique is readily compatible with existing fibre systems and requires minimal sample preparation, and the resulting devices are inherently contained inside a stable environment.

The field of ultrafast laser inscription (ULI) has matured since its inception in 1996 and is now a powerful technology for realising 3D integrated waveguide components for a number of applications. Significant advances have been made in quantum information science, laser sources, biophotonics, astrophotonics, sensing, metrology, and telecommunications. In the past 20 years, many research articles have been published in the field, either giving insight into the light-material interactions underlying the technique or demonstrating one of the multitudes of photonic components that have been fabricated. The reader is directed to these selected review articles for an overview [4–11].

One such component fabricated using this technique is of particular importance for many of the research fields mentioned above – that being the waveguide Bragg grating (WBG) [8, 12]. Analogous to a fibre Bragg grating (FBG) [13], a WBG consists of a periodic perturbation of the effective refractive index of the light guiding region inside a bulk material. This periodic perturbation (grating period) can be tailored to reflect particular wavelengths of light, centred at the Bragg wavelength, whilst transmitting all other wavelengths. ULI is well suited to the fabrication of WBGs as each grating period is individually

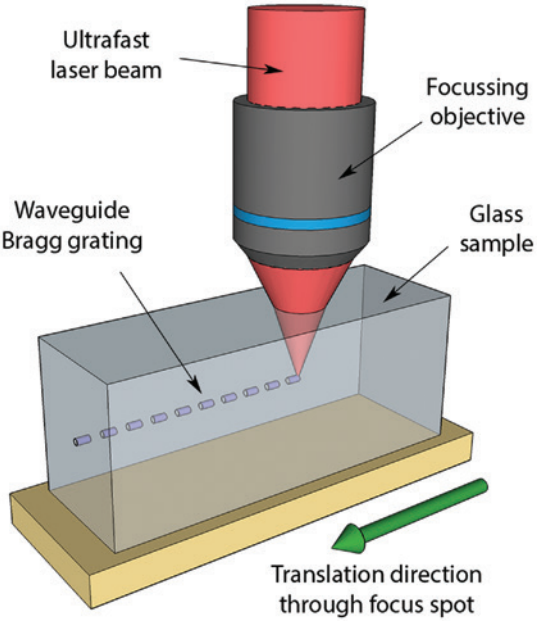


Figure 1: Schematic outlining ULI.

***Corresponding author: Martin Ams,** Centre for Ultrahigh Bandwidth Devices for Optical Systems (CUDOS), MQ Photonics Research Centre, Department of Physics and Astronomy, Macquarie University, Sydney, Australia, e-mail: martin.ams@mq.edu.au
Peter Dekker, Simon Gross and Michael J. Withford: Centre for Ultrahigh Bandwidth Devices for Optical Systems (CUDOS), MQ Photonics Research Centre, Department of Physics and Astronomy, Macquarie University, Sydney, Australia

BY-NC-ND ©2017, Martin Ams et al., published by De Gruyter.
This work is licensed under the Creative Commons Attribution-NonCommercial-NoDerivatives 3.0 License.

controlled during the writing process, and the restrictive use of a phase mask typically found in ultraviolet (UV) photoinscription methods is not required.

A distinguishing feature of gratings is their flexibility in achieving different spectral characteristics by tailoring the index perturbations. The grating period can be made uniform or graded and either localised or distributed in a superstructure. As such, grating structures find application in telecommunication networks (optical signal control), narrow linewidth lasers (wavelength stabilisation), and laser resonators (dispersion compensators and cavity mirrors). Furthermore, gratings can be used as direct sensing elements calibrated to a shift in their reflection/transmission spectra, thus allowing temperature and/or strain, for example, to be measured [14, 15].

In this review, we summarise the field of ultrafast laser-written WBGs over the past decade since its first report in 2006 [12]. The manuscript concentrates only on WBGs created via multiphoton, nonlinear excitation processes and not on those created using two-photon routes, namely, we focus on laser writing pulses in infrared and visible as opposed to UV. Moreover, we concentrate on WBGs fabricated inside bulk materials and point the reader to other review articles on the field of fibre-based ultrafast laser-written gratings [8, 16]. After outlining the various fabrication techniques in the next section, we then dedicate a section to describing how to tailor WBG characteristics. Following this are sections on the different WBG types and some applications demonstrated to date. The review is then summarised with concluding remarks.

2 WBG fabrication techniques

In this section, we outline the two main fabrication techniques that are used to create WBGs in bulk materials without the use of a phase mask.

2.1 Point-by-point (PbP)-based method

In 2006, Marshall et al. reported the first demonstration of a laser-written waveguide device integrated with a WBG [12]. The fabrication process involved in creating the WBG was based on the PbP method more commonly applied to the inscription of FBGs [17–19]. In the PbP method, each grating perturbation (or voxel) is individually created by a single laser pulse of sufficient energy, typically close to or just above the damage threshold of the sample. In general, systems running at low repetition rates (< 500 kHz) are used to generate the pulse energies required to achieve single PbP modifications. The waveguide and WBG created by Marshall et al. used a sequential direct-write process that passed over the same region twice. The waveguide was written before the grating structure and the WBG extended over the entire waveguide length (Figure 2A). A similar line-by-line approach to this PbP method was proposed in 2005 but never realised [20].

The reflection spectra of a typical waveguide and second-order WBG using this two-step process are shown in Figure 2B. Although the region of material modified during the WBG inscription process was smaller than the total volume of the waveguide, the guided mode overlap with the WBG was sufficient to introduce a pronounced resonant reflection at the Bragg wavelength of 1550.63 nm. As expected, the waveguide-only structure showed no evidence of a resonant feature.

Later that year, Zhang et al. showed that WBGs could be fabricated in alumino-borosilicate glass using the PbP method with only one scan of the writing pulses [21, 22]. In this case, the grating structure modifications were sufficient themselves to hold and propagate a light mode

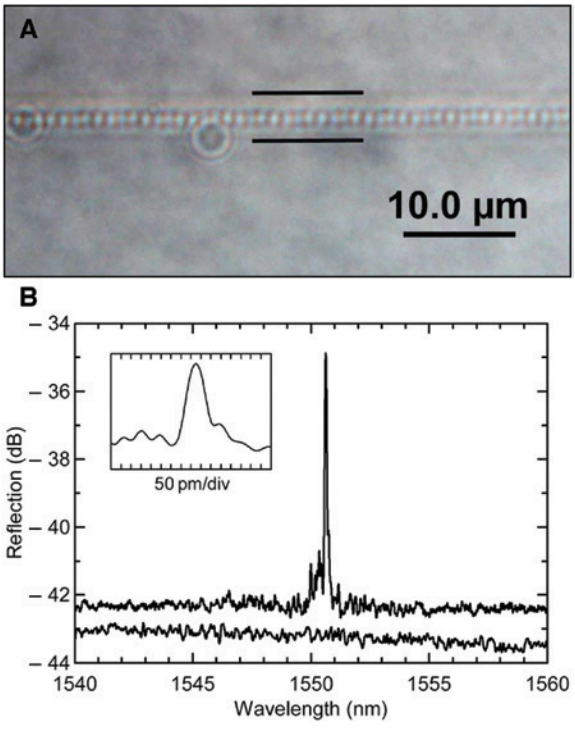


Figure 2: (A) Top-view image of a WBG fabricated in a fused silica sample. As a visual aid, the waveguide edges are indicated by horizontal black lines. (B) Reflection spectra from a PbP WBG (top curve) and a waveguide-only structure (bottom curve). The inset shows the WBG curve on an expanded abscissa. Reprinted with permission from [12].

without requiring an underlying waveguide structure. Under weak focussing conditions (0.25 NA), gratings based on type II modifications were created in the C-band and measured to have a maximum reflectivity of 36%. Type II material modification refers to optical damage of an irradiated sample [3]. Furthermore, various grating orders were realised and multiwavelength, serially cascaded WBGs were demonstrated (Figure 3). However, the trade-off between increasing WBG propagation loss (PL) and increasing grating strength limits the scope for low NA WBG fabrication.

By optimising the laser processing conditions, namely, pulse duration, pulse energy, and focusing geometry (0.55 NA), the same research group was able to find processing windows to create both low-loss and high-strength WBGs in the following year [23]. Grating responses in transmission varied from relatively weak (< 5 dB) dual-peaked lines when using short 100 fs writing pulse durations to strong (> 35 dB) single-peaked resonances using long 1 ps pulse durations. The two distinct Bragg resonances using 100 fs were due to pure TE and TM mode excitations giving rise to birefringent WBGs, whereas WBGs using 1 ps were birefringence free. This is not too surprising considering the laser-modified regions using 100 fs were very asymmetric (3 × 30 μm) due to self-focusing effects and spherical aberration.

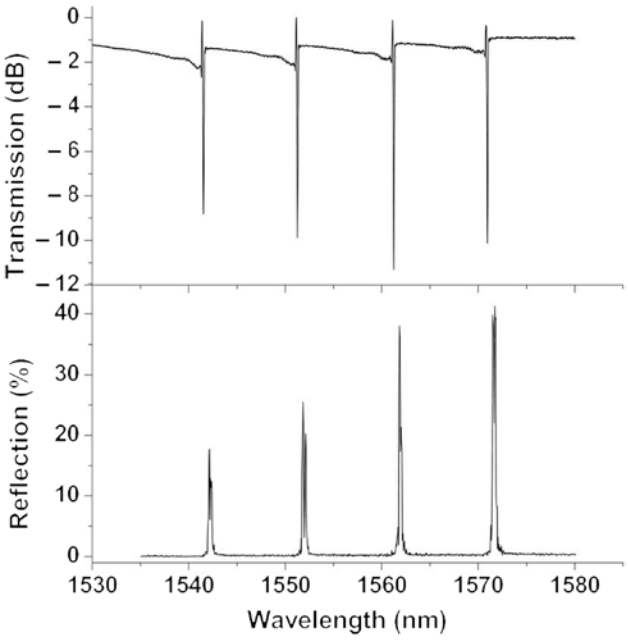


Figure 3: Spectra of four serially cascaded WBGs.
The different Bragg resonances were creating by slightly altering the sample translation speed during PbP fabrication. Reprinted with permission from [22].

Single-scan PbP WBGs have an inherently small size, giving rise to both pros and cons. Gross et al. took advantage of these small structures to successfully demonstrate the inscription of a first-order WBG at 800 nm with a period of 270 nm, the shortest reported to date [24]. In general, however, such small index dimensions are undesirable as the large difference in size between the physical modifications and guided mode results in relatively weak gratings. Another disadvantage of single-scan PbP WBGs is that they are typically based on type II modifications, which inherently increase the PL due to scattering.

A recent publication proposed a method to maximise the WBG refractive index using the PbP technique whilst also controlling the guided mode size to address some of these issues [25]. Waveguide bundles, consisting of multiple waveguides packed and overlapped into a homogeneous and symmetric hexagonal structure, surrounded a single central PbP WBG structure. Whilst the WBG index contrast may have been maximised, the PbP structures were still small compared to the surrounding hexagonal waveguide region (low modal overlap) and the resulting WBGs were quite lossy, relatively weak, and very broad.

2.2 Modulated burst method

To overcome the shortcomings of the PbP method, Zhang et al. adopted another fabrication approach, whereby multiple ultrashort laser pulses were used to form each refractive index voxel in the WBG structure [26]. A periodically segmented waveguide, or WBG, was created by modulating the ultrafast laser source to generate a burst of laser pulses. By selecting the modulation frequency and the sample translation speed, the refractive index perturbations can be tuned to yield sharp Bragg spectral resonances (Figure 4). This modulated, single-step fabrication approach provides greater control of the physical size and overlap of the refractive index voxels than the PbP method. Moreover, it opens an avenue for WBG fabrication using high repetition rate laser sources, where a very precise balance of pulse energy, writing speed, and interburst period is required [27–29].

There are a number of techniques that can be used to modulate the ultrafast laser source. Zhang et al. used an acousto-optic modulator (AOM) in the pulse train, which was driven by a controllable square waveform [26], whereas Chung et al. inserted a chopper to periodically block the writing beam [27]. Our group modified the technique such that the laser output was square-wave modulated in intensity by continuously interrupting the Pockels cell signal of the writing laser's amplifier cavity [28–30].

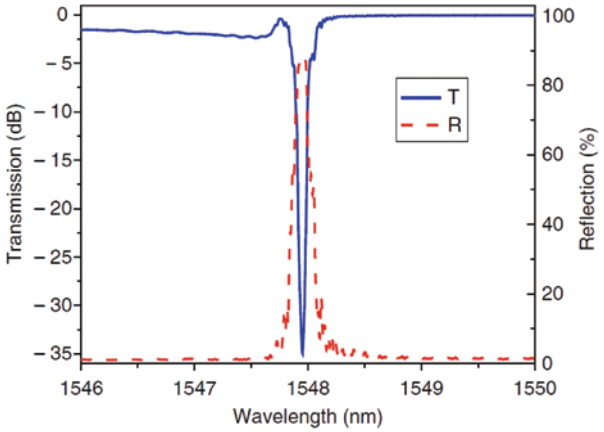


Figure 4: Transmission (T) and reflection (R) spectra of a WBG written in fused silica using the modulated burst method. Reprinted with permission from [26].

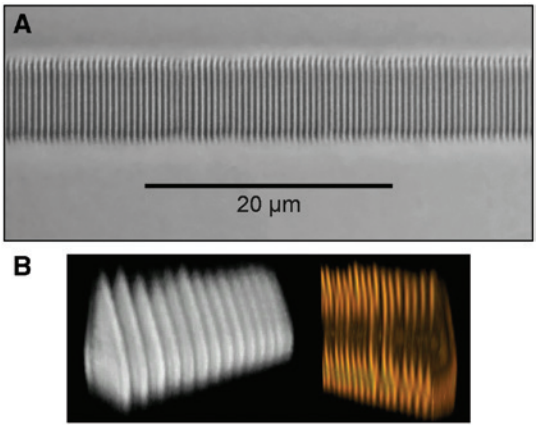


Figure 5: (A) Top-view transmission differential interference contrast (DIC) microscope image of a first-order WBG structure (period $\Lambda \approx 500$ nm) fabricated in a Kigre QX phosphate sample using the modulated burst method. (B) Third-harmonic generation (THG) image of a fourth-order WBG structure in the same sample using an adaptive-optical (AO) microscope [32]. The typical triangular cross-section of an index structure created using the slit method [33] is evident.

The pulse firing trigger signal was synchronised and locked to the encoder position feedback of the translation stages, thereby maintaining the phase between each successive grating perturbation. Not only can the relative phase between grating perturbations be maintained using this synchronisation, but also the absolute phase between multiple components can be precisely controlled. This was demonstrated by Ha et al. to fabricate symmetric and antisymmetric WBG couplers [31].

Example micrographs of C-band WBGs fabricated using the modulated burst method are shown in Figure 5. The refractive index perturbations and WBG shape are clearly shown using two different nondestructive imaging techniques.

3 WBG characteristics

The optical properties of a WBG are determined by the axial and radial variation of the induced refractive index change. In this section, we outline the most common quantitative WBG characteristics that arise from coupled-mode theory and only consider short period reflection Bragg gratings, where coupling is between tightly bound counterpropagating modes. See [13, 14, 34–36] for a more rigorous description of coupled-mode theory and grating construction.

3.1 Bragg condition

When a guided light wave enters a grating medium, it undergoes minute Fresnel reflections from the interface of every refractive index perturbation. If all the individual reflections are in phase, the many reflections combine with constructive interference and the medium reflects the incident wave over a narrow wavelength range. In the simple case of coupling between two counterpropagating guided modes by a uniform grating, the resonant wavelength for reflection where mode coupling is the strongest is given by the familiar Bragg condition [37]:

$$\lambda_B = 2\frac{n_{\text{eff}}\Lambda}{m} \tag{1}$$

where λ_B is the Bragg wavelength, n_{eff} is the effective modal index (also the average or DC refractive index) of the propagating mode, Λ is the period (or pitch) of the refractive index modulation, and $m = 1, 2, 3, \ldots$, is the diffraction, resonance, or grating order. It is important to note that only nonsinusoidal refractive index perturbations lead to higher-order WBG resonances, and in the case of a 50% duty cycle square-wave refractive index profile, only odd higher-order modes are reflected [14, 38–40]. This is due to the nature of the Fourier series expansion of the periodic index function. Duty cycle refers to the mark/space ratio of an individual grating perturbation.

Figure 6 shows the evolution of the Bragg wavelength with duty cycle for a number of WBG orders and a fixed sample length of 4 mm. As the duty cycle increases, the effective modal index grows linearly before eventually deviating from this trend at higher duty cycles. This is due

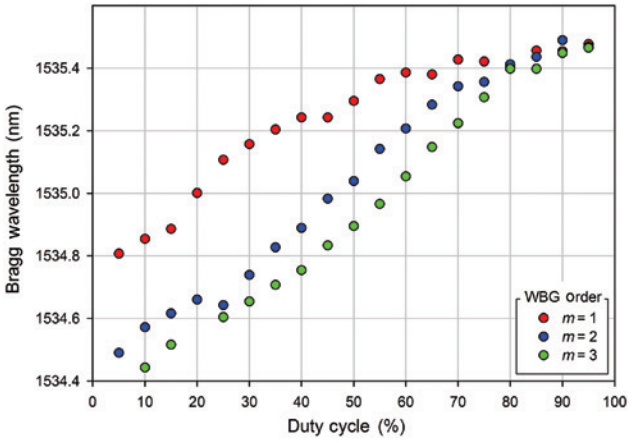


Figure 6: Bragg wavelength as a function of duty cycle for various WBG orders m.
WBGs were fabricated in a 4-mm-long silicate glass sample using the modulated burst method.

to the overlap of the individual index voxels and a saturation of the available refractive index modification.

3.2 Coupling coefficient κ

The coupling coefficient of a WBG's two counterpropagating guided modes κ is given by [13]

$$\kappa = \frac{\pi \Delta n_{AC}}{\lambda_B} g(z)\eta \tag{2}$$

where Δn_{AC} is the amplitude (or AC component) of the WBG index perturbations. A useful technique to control the strength of Δn_{AC} (and in turn κ) is through the duty cycle and writing pulse energy. Typical Δn_{AC} values for WBGs are in the range of 1×10^{-4} to 5×10^{-3}. The apodisation function $g(z)$ (typically of a constant, Gaussian, or raised-cosine weighting) can be used to control reflection side lobes, whereas η, the modal overlap factor, is the fraction of the guided mode field power within the physical cross-section of the WBG index perturbation. Techniques to control WBG cross-sections are outlined in a following section.

For finite uniform WBGs, the coupled-mode equations have an exact solution. By applying appropriate boundary conditions, the maximum reflectivity of a WBG (which occurs at the Bragg wavelength) of length L can be calculated from

$$R_{max} = \tanh^2(\kappa L). \tag{3}$$

The product κL is a measure of grating strength, where a WBG with $\kappa L > 3$ ($R > 99\%$) is termed a "strong grating". R_{max} can also be calculated from the transmission spectrum of the WBG using

$$R_{max} = 1 - 10^{-(T/10)} \tag{4}$$

where T is the absolute depth of the transmission notch in decibels (dB) at λ_B.

Figure 7 shows experimental coupling coefficients calculated using Equations (3) and (4) from a suite of 1535 nm WBGs fabricated in a silicate glass (Schott IOG-10) using the modulated burst method. Various duty cycles, WBG lengths, and orders are captured in these data. It should be noted that data could not be obtained for first-order WBGs with lengths greater than 4 mm, as the transmission depths were too strong (> 50 dB) to be resolved by our analysers.

First, Bragg resonances were realised for every grating order tested (which included odd and even higher orders), demonstrating that the refractive index profile of WBGs written using the modulated burst method does not follow a sinusoidal function [14, 38–40]. Furthermore, the grating strength for a first-order WBG peaks at a duty cycle of 35% (radiation mode losses dominate below duty cycles of 20%) and not the expected 50%, indicating that there is an offset between the desired WBG period and the resolvable pitch of the individual voxels. We also noticed a 35% duty cycle peak for first-order WBGs operating at 1030 and 725 nm (not shown). This offset matches what Zhang et al. reported [26]. The local minima and maxima seen for higher-order WBGs are due to the sinc function coefficients of the periodic Fourier expansion.

By fixing the duty cycle at 35% and scanning through fabrication pulse energies for a number of first-order Bragg

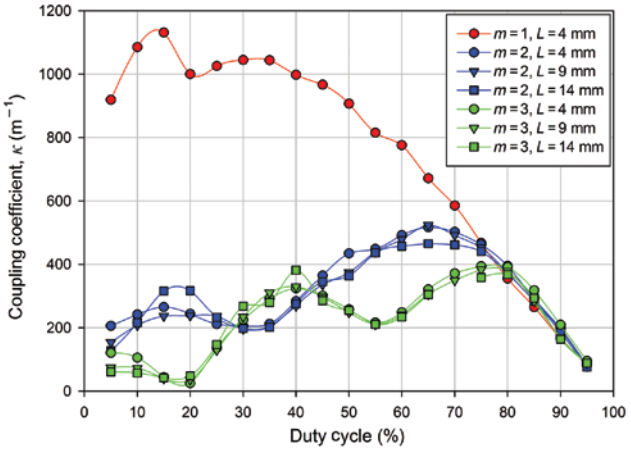


Figure 7: Coupling coefficients κ of C-band WBGs fabricated in a silicate glass (Schott IOG-10) using the modulated burst method. Various duty cycles, WBG lengths (L), and orders (m) are shown.

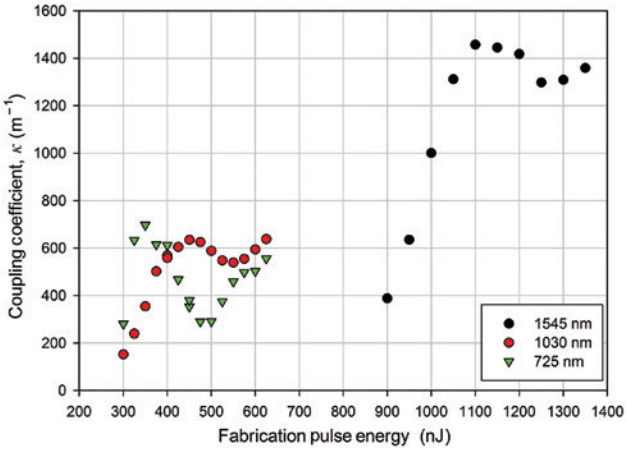


Figure 8: Coupling coefficients κ of first-order WBGs fabricated in a 4-mm-long silicate glass (Schott IOG-10) at different Bragg wavelengths λ_B.
The duty cycle was fixed at 35%, whereas the writing pulse energy was varied.

wavelengths (Figure 8), it can be seen that κ varies not only with pulse energy but also with wavelength. The wavelength dependence is due to the trade-off between η and Δn_{AC}; however, we have no explanation as to why there are local minima and maxima with respect to pulse energy. Gross et al. also noticed this when writing visible WBGs with the PbP method and attributed it to a modal overlap change between two regions of index change above and below the individual void voxels [41]. As there is only one modification region for WBGs created in silicate glass using the modulated burst method, this explanation does not apply.

To compare WBGs with varying lengths, sample hosts, and fabrication techniques, researchers must compare κ values (which are quoted in units of inverse length). Unfortunately, many groups have made the mistake of simply comparing grating transmission depths divided by a constant to reach a common length as a measure of grating strength. For comparison, Table 1 lists κ values for

Table 1: Coupling coefficient κ and PL of WBGs fabricated by different research groups using the ULI technique. For comparison, the typical value of κ for standard UV-written FBGs in photosensitive fibre range from 150 to 300 m^{-1}.

Substrate	Fabrication technique	λ_B (nm)	κ (m^{-1})	PL (dB/cm)
Fused silica [12]	Two-step PbP	1550	131	–
Boro-aluminosilicate (Eagle2000) [21]	PbP	1551	25	–
Boro-aluminosilicate (Eagle2000) [22]	PbP	1551	145	0.6
Boro-aluminosilicate (Eagle2000) [23]	PbP	1550	472	0.5
Soda-lime [27]	Two-step PbP	1577	14	–
Fused silica [26]	Modulated burst	1548	111	1.5
Er:Yb codoped phosphate [30]	Modulated burst	1537	242	–
Yb-doped phosphate [42]	Modulated burst	1535	221	–
Boro-aluminosilicate (Eagle2000) [31]	Modulated burst	1551	713	–
Fused silica [43]	Modulated burst	1546	36	0.7
Boro-aluminosilicate (Eagle2000) [24]	PbP	799	65	–
Boro-aluminosilicate (Eagle2000) [28]	Modulated burst	1552	157	–
ZBLAN [29]	PbP überstructure	1550	324	–
Boro-aluminosilicate (Eagle2000) [44]	Multiscan modulated burst	1563	177	–
$LiNbO_3$ [45]	Modulated burst stressors	1540	45	–
Boro-aluminosilicate (Eagle2000) [41]	PbP	648	136	–
Boro-aluminosilicate (Eagle2000) [41]	PbP	698	183	0.8
Boro-aluminosilicate (Eagle2000) [41]	PbP	748	187	–
Boro-aluminosilicate (Eagle2000) [41]	PbP	798	163	–
Fused silica [46]	Modulated burst	1550	210	2.2
Fused silica [47]	Modulated burst	1549	280	<1
Chalcogenide (GLS) [48]	Modulated burst	1551	179	–
$LiNbO_3$ [49]	Multiscan modulated burst (depressed clad)	1558	1230	1.52–3.51
Boro-aluminosilicate (Eagle2000) [50]	Two-step PbP	1545	120	–
Fused silica [25]	PbP (waveguide bundle)	840	126	–
Fused silica [25]	PbP (waveguide bundle)	1550	220	1.6
Borosilicate (AF45) [51]	Modulated burst	1030	848	1.6
Silicate (this manuscript)	Modulated burst	1545	1457	0.22
Silicate (this manuscript)	Modulated burst	1030	634	–
Silicate (this manuscript)	Modulated burst	725	696	–
Borosilicate (AF45) (this manuscript)	Modulated burst	643	314	–

a variety of WBGs fabricated by different research groups using the ULI technique.

3.3 Bandwidth

Another important property of a WBG is its bandwidth, which is a measure of the wavelength range over which the WBG reflects light. The bandwidth of the reflection peak can be measured at its full-width at half-maximum (FWHM). However, a more readily calculated bandwidth is that between the first zeros on either side of the reflection peak. By calculating the difference in propagation constants between the first zeros and λ_B, the bandwidth is given by [36]

$$\Delta\lambda = \frac{\lambda_B^2}{n_{\text{eff}}}\sqrt{\frac{\kappa^2}{\pi^2}+\frac{1}{L^2}}. \tag{5}$$

From Equation (5), it follows that the bandwidth of weak WBGs ($\kappa L < 1$) are length limited, such that a longer grating has a narrower bandwidth. In contrast, for strong WBGs ($\kappa L > 3$), the light does not penetrate the full length of the grating; thus, the bandwidth is directly proportional to the coupling coefficient and is almost independent of length. Therefore, by reducing κ, it is possible to narrow the linewidth of a strong WBG.

Due to the distributed nature of the reflection process in a WBG, the incident wave penetrates a certain distance into the grating before reemerging at the front end. This effective distance, at λ_B, is known as the penetration depth and can be approximated for small refractive index changes as [52, 53]

$$D = \frac{\tanh(\kappa L)}{2\kappa}. \tag{6}$$

Figure 9 shows that the bandwidth of C-band WBGs fabricated using the ULI technique can be tailored by carefully selecting the WBG length, strength (by varying κ through the duty cycle), and order.

3.4 WBG cross-section

The cross-section of a WBG, and in turn the modal overlap factor η, plays an important role in determining the strength of a grating. Beam shaping techniques used to manipulate the cross-section of femtosecond laser-written waveguides can be found in [10]. This section outlines those relevant to the fabrication of WBGs.

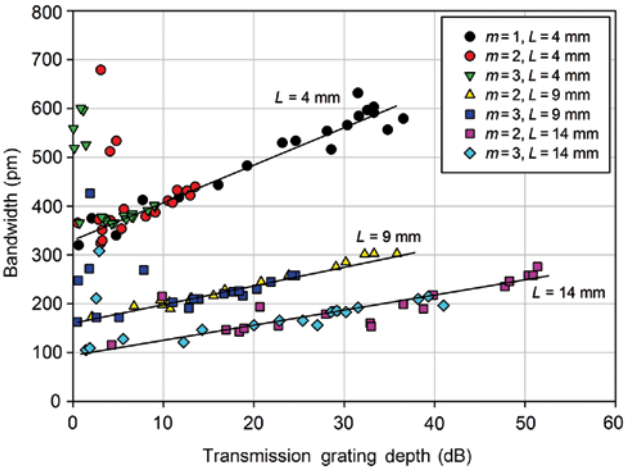


Figure 9: C-band WBG bandwidth as a function of grating depth for various WBG orders (m) and lengths (L).
Each data point represents a different duty cycle. WBGs were fabricated using the modulated burst method in a silicate glass.

We employ the slit method to finely control WBG cross-sections [33]. The resulting index profiles are typically triangular in shape (Figure 5) and guide circularly symmetric modes [32, 54, 55]. The limitation of the slit method is that, to generate large modified areas, low NA focussing objectives are required, which makes it difficult to achieve short-pitched gratings.

Brown et al. showed that the multiscan technique can be used to create WBG cross-sections with a step-like index profile [44]. The technique is flexible; however, every laser scan must be in phase to generate a resonant response.

In situations where a material responds with a negative index change during inscription, depressed cladding arrangements are typically used to control waveguide cross-sections [3]. Gross et al. demonstrated that WBGs consisting of periodic planes, constructed from a transverse hexagonal lattice of smaller point features, can be created inside a depressed cladding waveguide structure to control η (Figure 10) [29]. Kroesen et al. combined the multiscan technique and a cladding arrangement based on type II modifications to increase the WBG modal overlap factor [49]. Both the multiscan technique and the depressed cladding approach suffer from inflated fabrication times, and the increased number of inscription scans also subjects the WBG to changing environmental conditions during fabrication.

High repetition rate lasers, operating in the cumulative heating regime, enable the simple control of a waveguide's cross-sectional dimension [56, 57]. The index profile is typically complex, consisting of regions of both positive and negative contrast [58, 59]. However, WBGs

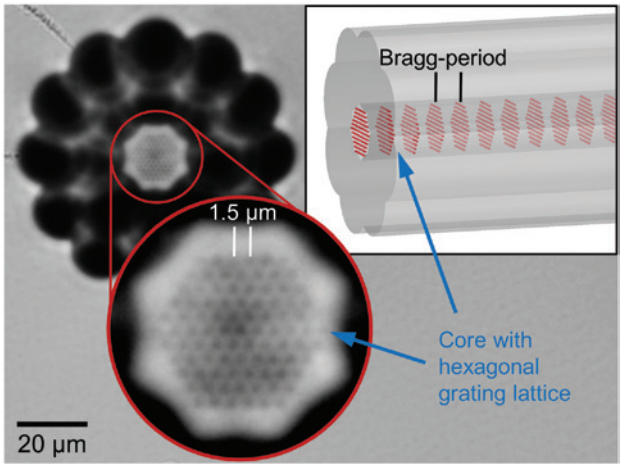


Figure 10: End on, bright-field microscope image of an überstructure WBG revealing the hexagonal lattice of point features within the core of the waveguide.
The inset shows a 3D render of the structure (not to scale).
Reprinted with permission from [29].

created in the cumulative heating regime rely on the formation of nanosized voids, whose cross-sectional dimension cannot be controlled [28].

3.5 WBG loss

The amount of light lost through an optical device is a key parameter that needs to be included in any specification of the device. WBGs fabricated in passive hosts using ULI possess three main sources of loss: Fresnel loss, coupling loss (CL), and PL. The insertion loss (IL) or out-of-band loss (on the long wavelength side of λ_B) is the sum of all these losses. The IL is simply the ratio of the measured transmitted powers with and without the WBG included in a fibre-to-fibre coupling setup. Index matching gel or oil is typically applied to all air-glass interfaces in this setup, with matching refractive indices, to mitigate Fresnel losses leaving only the CL and PL to be calculated.

The CL accounts for the mode mismatch (power loss when coupling from one mode to another due to the mismatch in the transverse electric field distribution) that occurs between optical fibres and WBG inputs and outputs. The CL can be estimated by evaluating the appropriate overlap integrals of the coupling efficiency formula [60] using the near-field mode profiles of fibres and WBGs captured with a CCD camera.

The PL is the loss remaining once the CL has been subtracted from the IL. In high index materials, the Fabry-Perot resonance technique can be used as an alternative to measure the PL of optical devices [61]. The PL can also be determined by taking the appropriate difference between the IL of different length devices written under identical conditions (i.e. the cut-back method). This method assumes an identical CL, therefore leaving the PL as the only remaining source of loss. Figure 11 shows the PL and CL (calculated using the cut-back method) of different order C-band WBGs fabricated in a silicate glass with a fixed pulse energy and various modulated burst duty cycles. Single-mode SMF-28 was used as the coupling fibre.

The PL at 1535 nm is fairly constant and averages to 0.22 dB/cm. The scatter in the data is due to the limited number of sample lengths tested (3 in this case) and the inability to achieve the exact same coupling conditions with each different length sample. These later two points highlight potential drawbacks of the cut-back method but turn out not to be significant in our results. It is interesting

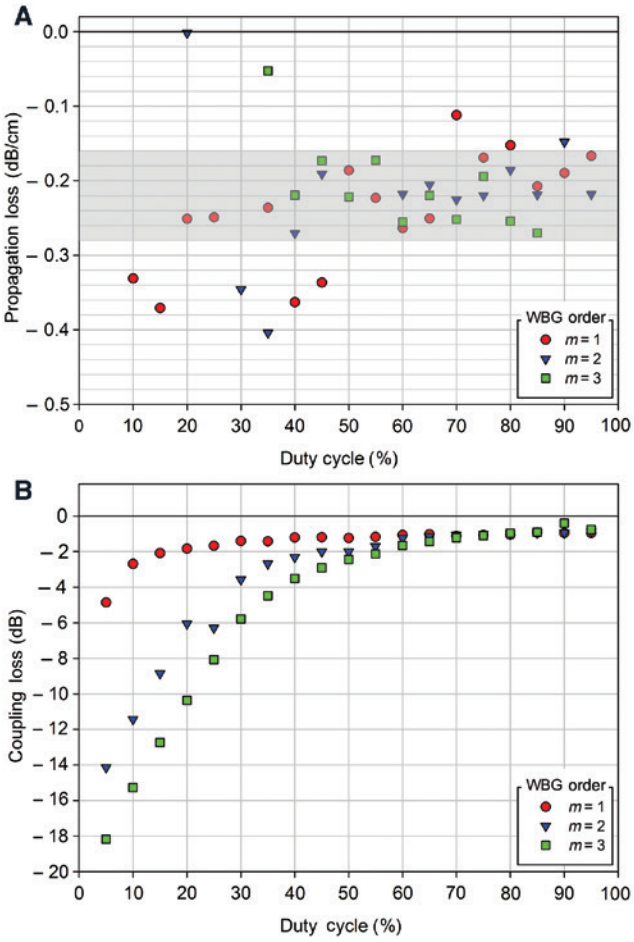


Figure 11: (A) PL and (B) CL of C-band WBGs calculated from three different length samples using the cut-back method.
WBGs were fabricated in a silicate glass sample using the modulated burst method. Single-mode SMF-28 was used as the coupling fibre. The shaded region provides an average visual guide.

to note that, in contrast to the results shown in Figure 11A, Zhang et al. reported a strong decrease in the PL with increasing duty cycle, attributing this to a reduction in scattering by a deepening Δn_{AC} [26]. For comparison, Table 1 lists the PL values for a variety of WBGs fabricated by different research groups using the ULI technique.

The CL in Figure 11B clearly changes with duty cycle due to the guided WBG mode size being dependent on n_{eff}. As the duty cycle decreases, n_{eff} decreases causing the WBG mode size to grow, thus decreasing the amount of light coupled to and from the SMF-28 fibre mode. In these results, the CL is at least five times higher than the respective PL for any given duty cycle, which is effectively the majority of the overall IL. Hence, by engineering the WBG cross-section and n_{eff} appropriately, it should be possible to reduce the IL to that of only the PL.

Another inherent source of loss in a WBG is the gradual decrease in transmission leading up to the Bragg resonance from the short wavelength side, which can be seen in both Figures 3 and 4. This smooth transition profile demonstrates loss due to coupling of the core mode to a continuum of radiation modes. This contrasts with the usually discrete FBG cladding mode structure and is due to the WBG geometry having no well-defined cladding [39]. Although radiation mode losses inhibit the number of WBGs that can be serially cascaded next to one another, their strength can be somewhat controlled. Zhang et al. found that WBGs fabricated using the modulated burst method have a ≈ 2 dB radiation mode loss, which is much less than the >5 dB loss associated with WBGs formed by the single-pulse PbP method [8]. We also observed that a reduction in radiation mode loss can be achieved by increasing the WBG duty cycle.

3.6 Birefringence

Birefringence is an optical property whereby a material's refractive index varies with the polarisation direction of light. If a WBG is birefringent, there will be a different Bragg resonance peak associated with each polarisation axis. The multiple Bragg resonances may be evident when probed by an unpolarised light source; however, if the birefringence is low, they may not be able to be resolved and a polarised probe source will need to be used for each polarisation axis. The difference in these Bragg wavelengths can be used as a means to determine the degree of birefringence using the following relation:

$$\Delta n_B = \frac{\lambda_{B2} - \lambda_{B1}}{2\Lambda}. \quad (7)$$

WBG birefringence may arise from the choice of substrate [49], laser-induced stresses [62], asymmetric waveguide modes [23], or self-aligned nanogratings [63, 64]. The ULI technique gives researchers access to pathways of birefringence manipulation, thus opening an avenue to creating 3D polarisation-dependent/independent optical circuits.

The simplest way to generate a large WBG birefringence is to choose a birefringent host material from the outset. Kroesen et al. used lithium niobate to create WBGs with a birefringence of 3.5×10^{-2} [49]. The majority of WBG demonstrations, however, have been reported in low birefringent materials.

In a boro-aluminosilicate glass, Zhang et al. used 100 fs laser pulses and the PbP technique to produce relatively weak dual-peaked WBG responses [23]. These two distinct Bragg resonances, shown in Figure 12, are due to birefringence (1.9×10^{-4}) created from very asymmetric (3×30 μm) laser-modified regions. Using the multiscan modulated burst method, Brown et al. also created birefringent WBGs (3.8×10^{-4}) in a borosilicate glass [44].

In subsequent experiments, Zhang et al. reported birefringent WBGs (3.2×10^{-4}) in fused silica using the modulated burst method and a linearly polarised writing beam aligned perpendicular to the direction of sample translation [26]. The dependence of birefringence on the polarisation of the inscription beam was further examined by Fernandes et al. who reported birefringence values of 5.5×10^{-5} and 2.1×10^{-4} at 1550 nm for parallel and perpendicular writing polarisations, respectively [65]. The larger birefringence associated with the perpendicular alignment also corresponded to an increase in the PL in the fused silica sample.

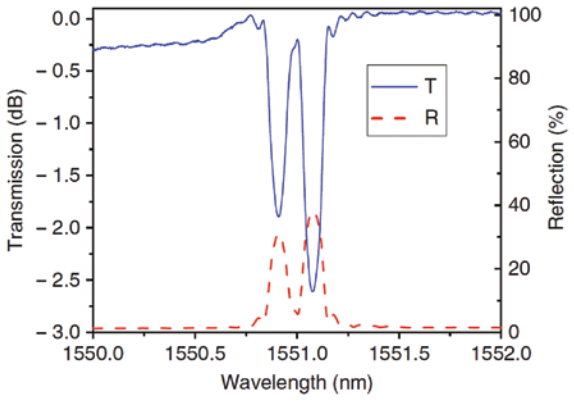


Figure 12: Spectral response of a PbP WBG written in boro-aluminosilicate glass.
Peak splitting corresponds to a WBG birefringence of 1.9×10^{-4}.
Reprinted with permission from [23].

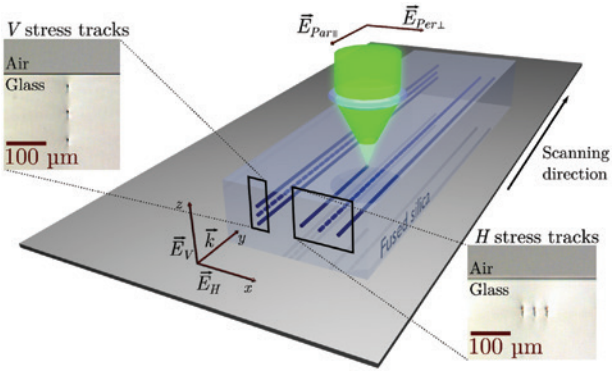


Figure 13: Stressed WBG fabrication, where $\vec{E}_V$ and $\vec{E}_H$ indicate the electric field orientation for vertical (*V*) and horizontal (*H*) waveguide polarisation eigenmodes.
$\vec{E}_{Par\parallel}$ and $\vec{E}_{Per\perp}$ represent the parallel and perpendicular polarisations of the writing laser, respectively. The insets show microscope end-on images of WBGs sandwiched with vertical (left) and horizontal (right) stress tracks. Reprinted with permission from [62].

To preferentially stress and tune existing WBG birefringence, Fernandes et al. fabricated parallel laser modification tracks, also known as stressors, around WBGs in fused silica [62] (Figure 13). Maximal change was obtained by placing the stressors as close to the WBG as possible without inducing coupling between the WBG and stressor tracks. By fabricating stressors 20 µm above/below the WBG mode (along the inscription axis) using a parallel linearly polarised inscription beam, the birefringence was reduced from 6.6×10^{-5} to 1.5×10^{-5}. Stressors placed 13 µm on either side of the WBG using a perpendicular linearly polarised writing beam increased the birefringence up to 4.35×10^{-4}.

Similarly, stress tracks written 13 µm to either side of a WBG but with a circularly polarised beam (of pulses stretched to 400 fs) generated the maximum birefringence (5×10^{-4}) in a silicate glass (Schott IOG-10) without affecting the guided mode profile (Figure 14). The initial WBG birefringence without stress tracks was 2×10^{-5}.

3.7 Annealing stability

WBGs show potential application in telecommunications, sensing, and as laser sources where high stability and longevity are required. Testing these characteristics typically involve subjecting WBGs to various annealing and accelerated lifetime studies. Zhang et al. exposed PbP-written WBGs in boro-aluminosilicate and modulated burst-written WBGs in fused silica to several heating cycles up to 750°C and 1000°C, respectively [23, 66]. In both cases, there was very little WBG degradation up to 500°C, with only a slight decrease in grating depth and small increase in the mode field diameter (MFD), indicating a reduced effective refractive index. In the boro-aluminosilicate glass, mode confinement was no longer observable beyond 750°C as the strain point of 666°C was exceeded. In fused silica, the MFD increased by 50%, the PL more than tripled, and the grating depth dropped by 27 dB after treatment at 750°C . Waveguiding ceased after 1000°C, a value that is higher than the 893°C strain point for fused silica. It was concluded that, as a result, modulated burst-written WBGs in fused silica are preferred for high-temperature applications. Thiel et al. contrastingly showed that PbP WBGs fabricated in fused silica were only stable up to 250°C [25].

Dekker et al. fabricated WBGs in both doped and undoped phosphate glasses and used them as a diagnostic for monitoring subtle changes in the induced refractive index during photoannealing and thermal annealing experiments [67]. It was found that the grating depth reduced over time, the Bragg wavelength blue shifted, and the MFD of the WBG increased. This was attributed to a reduction in both n_{eff} and Δn_{AC} and was shown to be both wavelength dependent and dopant level dependent. For both doped and undoped phosphate samples, photoannealing arose due to the absorption of visible light, resulting in the annihilation of colour centres induced during the femtosecond inscription process akin to that observed in photosensitive fibres [15]. Although these colour centres are susceptible to photobleaching, they are thermally robust up to 70°C. In contrast, WBGs in a doped silicate glass host were shown to have improved optical properties during photoannealing experiments. In this case, the WBG refractive index contrast was photostable [68]. Waveguide lasers (WGLs) using this glass host showed a

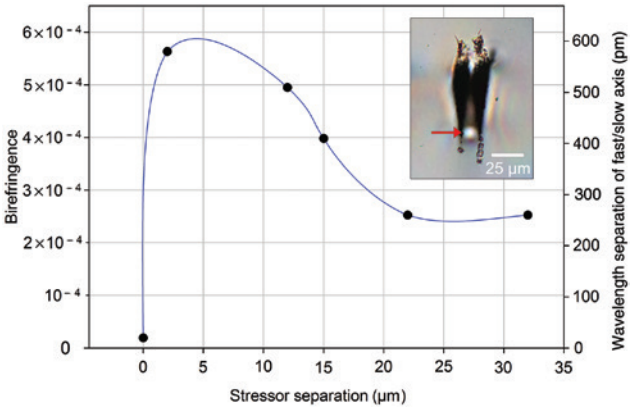


Figure 14: WBG birefringence induced by neighbouring stress tracks written with a circularly polarised beam in a silicate glass. The inset shows 13 µm spaced stressors written with 400 fs, 5 µJ, 1 kHz pulses surrounding a WBG under bright-field illumination. The arrow indicates the location of the WBG.

reduced threshold and increased output power over time due to a reduction in the PL.

Multiscan WBGs were inscribed in lithium niobate very close to the threshold between types I and II modifications by Kroesen et al. [49]. It was shown that, after thermal treatment at 250°C for 24 h, the WBG reflectivity decayed slightly; however, the spectral properties improved. The undesired side lobes cleared out, the reflection spectrum became more symmetric, and the transmission improved for both polarisations. Moreover, no deterioration of the WBG performance was observed within a time period of several months after annealing.

4 WBG types

In previous sections, we have only discussed the simplest form of a WBG, that is, a uniform WBG where the coupling coefficient and the grating pitch are constant along the grating length. Variations in either of these characteristics as a consequence of the fabrication conditions or by design result in non-"ideal" WBGs that can be tailored for specific applications. Examples of other common WBG types include apodised, chirped, phase shifted, and sampled as illustrated in Figure 15.

4.1 Apodised

Uniform WBGs of finite length result in reflection spectra with strong side lobes surrounding the central Bragg resonance peak. By apodising the coupling coefficient of the WBG, these side lobes can be suppressed [69]. Apodisation is achieved by varying κ spatially along the WBG length through the function $g(z)$ in Equation (2).

However, if the apodisation is accompanied by a DC refractive index change and thus a change in n_{eff} of the guided mode, the reflection spectrum becomes asymmetric around λ_B and side lobes reappear. A negative DC index change causes side lobes to occur on the long wavelength side, whereas a positive DC index change results in side lobes on the short wavelength end. Apodised gratings are used to reduce interchannel interference in dense wavelength-division multiplexed (DWDM) communications systems and can also be used to achieve the often-desired "top-hat"-like reflection.

Voigtländer et al. [70] and Zeil et al. [47] reported the single-step fabrication of Gaussian apodised WBGs in fused silica using the ULI technique. The apodisation of κ was accomplished by changing the duty cycle of the 500 kHz femtosecond pulse train. A reduction of the duty cycle changes n_{eff} of the waveguide; therefore, additional bursts of pulses were introduced in the off-periods so that the total number of writing pulses and n_{eff} was kept constant over a grating period. This approach required a dynamic adjustment of the pulse timing during the fabrication process. Using this technique, Zeil et al. obtained 13 dB sideband suppression in a 10-mm-long 35% reflective WBG; however, due to random small phase or amplitude fluctuations, higher-order side bands were lifted, reducing the overall sideband suppression to 10 dB (Figure 16).

Gross et al. used a two-step method to achieve Gaussian apodisation by inscribing a PbP WBG diagonally across a prefabricated waveguide [41], a process similar to one previously demonstrated in optical fibre [71]. Increasing the distance between the waveguide centre and the WBG modification decreases κ due to a decrease in overlap between the guided mode and the WBG. As the guided mode profile was Gaussian, κ varied with an approximately Gaussian dependence from the centre

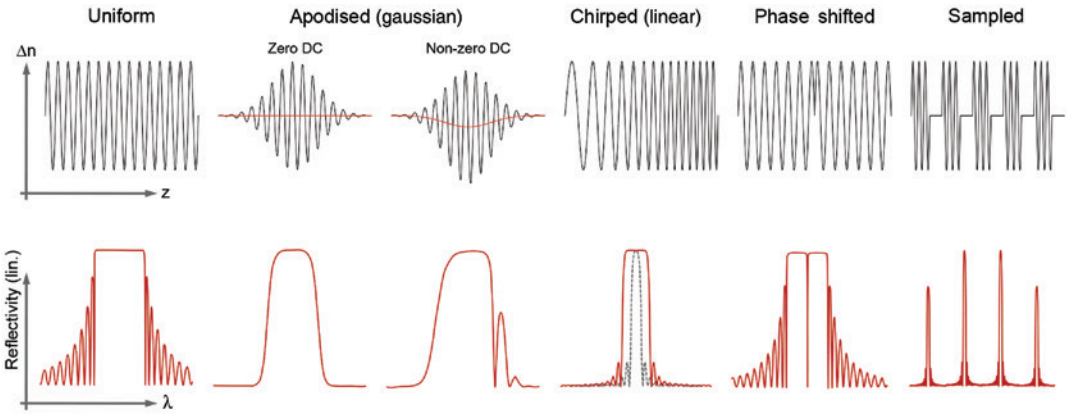


Figure 15: Illustrations of various refractive index modulations and their resulting reflection spectra.
The red lines in the refractive index profiles for the Gaussian apodised gratings indicate the average refractive index change.

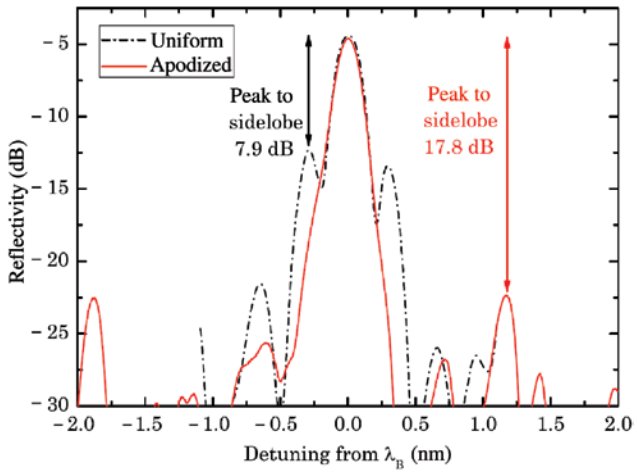


Figure 16: Comparison of a 4.4-mm-long uniform WBG and an apodised WBG employing a Gaussian apodisation function with 4.4 mm FWHM (10 mm total length).
WBGs were both fabricated in a fused silica sample using the modulated burst technique. Reprinted with permission from [47].

of the waveguide. Relative to the peak reflectivities, the two-step apodised WBG resulted in 7.3 dB side lobe suppression; however, it was only single sided, implying that the WBG also induced a DC refractive index change. Because only the side lobes on the short wavelength end were reduced, it was inferred that the DC refractive index change was negative, which is consistent with the presence of microvoids within a PbP-written WBG structure.

4.2 Chirped

Chirped Bragg gratings have been widely investigated in optical fibres and are probably the simplest variation of the uniform grating. In this case, a constant variation in the grating pitch along its length results in a broadening of the grating spectral response and a reduction in its reflectivity.

The simplest method to create a linearly chirped WBG using ULI is by accelerating the sample translation speed during inscription. The acceleration needed to obtain a targeted grating bandwidth $\Delta\lambda$ can be calculated by the starting (v_1) and finishing (v_2) velocities needed to generate the Bragg wavelengths at the ends of the desired spectrum according to

$$a = \frac{(v_2^2 - v_1^2)}{2Lv_1} = \frac{\Delta\lambda f}{4n_{\text{eff}}L}. \tag{8}$$

where f is the frequency of the modulated burst pulse train used to fabricate the WBG.

Using this approach with a duty cycle of 60%, Zhang et al. fabricated chirped WBGs centred at 1550 nm with bandwidths that varied from 190 pm to 18.22 nm (Figure 17) [72, 73]. For a fixed grating length of 25 mm, the effective reflectivity fell from 95% to 8% for the broadest grating. As the bandwidth increased, the centre wavelength decreased (reduced n_{eff}), whereas the PL increased.

Another approach to obtain linear chirped WBGs is to keep the sample translation fixed whilst varying the modulation frequency of the writing beam along the WBG. This approach was taken by Dolgaleva et al. who used a linearly chirped grating to take the temporal Fourier transform of an incident optical pulse [43]. A chirped WBG can perform a temporal Fourier transform of an optical signal if it has a sufficient amount of dispersion. A commonly used estimate of dispersion in a linearly chirped grating is

$$d_\rho = \frac{2n_{\text{eff}}}{c}\left(\frac{d\lambda_B}{dz}\right)^{-1} (\text{ps/nm}) \tag{9}$$

where the "chirp", $\frac{d\lambda_B}{dz}$, is a measure of the rate of change of the design wavelength with position in the grating, usually given in units of nanometers/centimeters. The chirped WBG was 5 cm long and had a bandwidth of 10 nm, dispersion coefficient of 34.8 ps/nm, and maximum reflectivity of 80%. The reflectivity, however, was heavily skewed to shorter wavelengths (80% compared to 20% at the long wavelength edge) due to higher PL for those wavelengths that travel longer distances through the device. Nonetheless, the simulated and experimental temporal Fourier transform results correlated well.

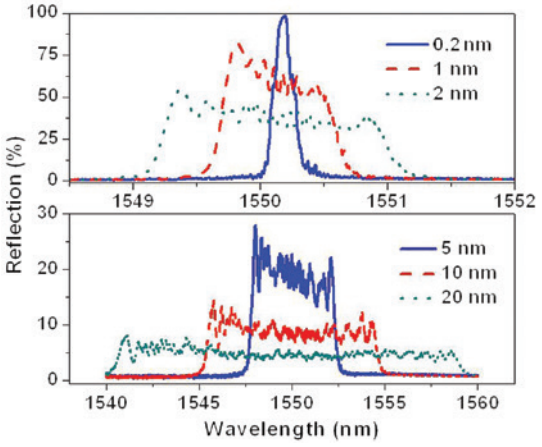


Figure 17: Reflection spectra of chirped WBGs fabricated using the modulated burst method in a fused silica sample.
Reprinted with permission from [72].

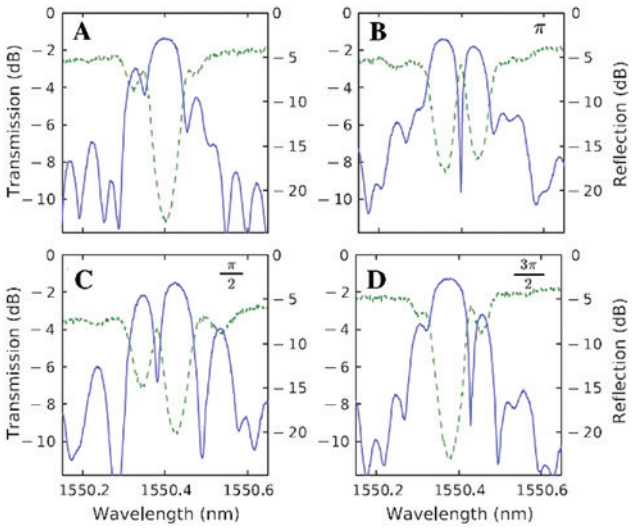


Figure 18: Vertically polarised transmission (dashed green curve) and reflection (solid blue curve) spectra for a fused silica WBG with (A) no phase shift, (B) π phase shift, (C) $\pi/2$ phase shift, and (D) $3\pi/2$ phase shift.
Reprinted with permission from [76].

4.3 Phase shifted

The addition of a discrete, localised phase shift in the centre of a uniform grating can be used to open up an extremely narrow transmission window in reflection whose position depends on the magnitude of the phase shift. Phase shifts can be used to tailor the shape of a passive grating filter or for channel selection in telecommunications. Another common example is a π phase shift positioned in the centre of a distributed feedback (DFB) laser. In this arrangement, single-mode lasing is favoured, as the phase shift breaks the threshold condition degeneracy of the two lowest-order laser modes [74].

The ULI technique is well suited to the incorporation of phase shifts due to the addressability of each individual refractive index voxel of the WBG. For example, placing a π phase shift in the centre of a 1550 nm WBG requires an approximate 250 nm offset between index perturbations, which can be obtained using typical high-resolution air-bearing stages with resolutions less than 4 nm. This level of control was demonstrated by Ams et al. where a phase shift was inserted at the centre of a 20-mm-long WBG fabricated in Yb-doped phosphate glass to open up a >15 dB notch in transmission [75].

Grenier et al. demonstrated passband control using various phase shift values located in the centre of a WBG (Figure 18) [76]. The narrow transmission band of the π phase-shifted WBG had a contrast of 15 dB in reflection and a 3 dB bandwidth of 22 pm (quality factor $Q = 70{,}455$) but could only be observed under polarised probing due to WBG birefringence. Grenier et al. also demonstrated a rectangular 200 pm passband in a WBG by cascading six π phase changes along the WBG at different locations.

4.4 Sampled

WBGs with a periodic "superstructure" imposed on their refractive index modulation are known as sampled gratings. Such a superstructure can be constructed by either varying κ, n_{eff}, or the grating pitch at intervals with a period much larger than the nominal grating period. Sampled gratings exhibit side-band resonances that are equally spaced in frequency about the fundamental resonance resulting in a comb-like spectrum [36]. Sampled gratings have been proposed and demonstrated for a number of applications including signal processing, tunable lasers, and wavelength reference standards in DWDM systems [14].

If the period of the sampled modulation in the WBG is Λ_s, the wavelength spacing of the side-band peaks is given by [77]

$$\Delta\lambda_s \approx \frac{\lambda_B^2}{2n_{\text{eff}}\Lambda_s}. \tag{10}$$

The strengths of the side-band resonances are approximately determined by the magnitude of the modulated superstructure's Fourier harmonics and naturally follow a sinc envelope. In the simplest case of a 50% duty cycle square-wave modulation, the side-band resonances occur at odd-integer multiples of $\Delta\lambda_s$. Furthermore, in a periodically phase-modulated sampled grating, the fundamental Bragg resonance is suppressed, and the equally spaced side-band resonances emerge about the depleted Bragg resonance.

Ams et al. took this approach to create a sampled WBG in a doped phosphate glass sample using the ULI technique [75]. The authors periodically inserted a phase shift every 300 Bragg periods along the length of a WBG, resulting in a transmission spectrum where the Bragg resonance was suppressed and odd harmonic side-band resonances emerged every 5 nm (Figure 19). When the structure was optically pumped to inversion, dual-wavelength laser operation was achieved at the first-order side-band resonances.

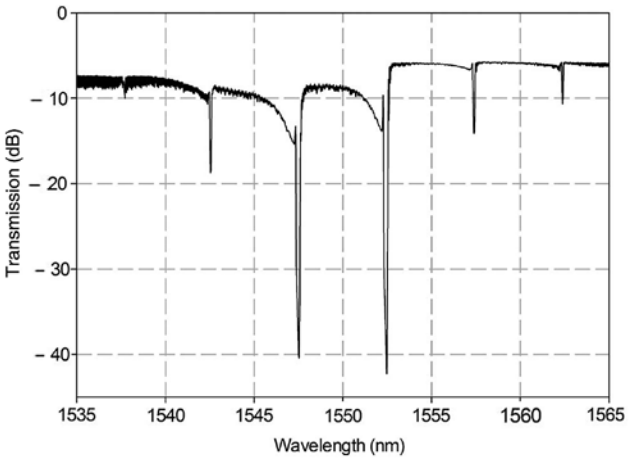


Figure 19: Transmission spectrum of a phase-modulated sampled WBG fabricated in Yb-doped phosphate glass using the modulated burst ULI method.
The central Bragg resonance is suppressed, whereas odd harmonic sideband resonances emerge. The complex grating structure was written in a single fabrication step without any postprocessing. Reprinted with permission from [75].

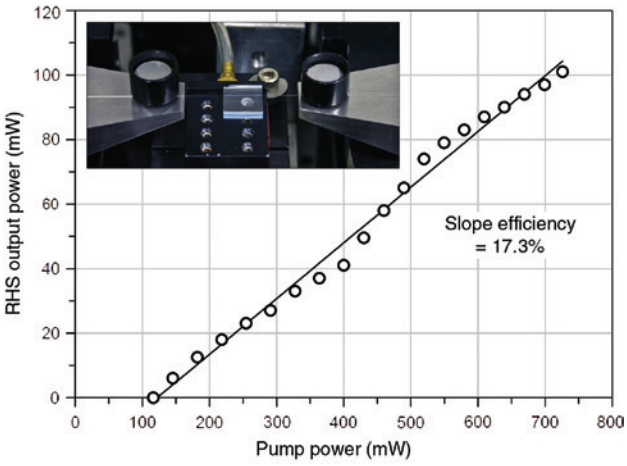


Figure 20: DFB WGL at 1032 nm fabricated in a 9% Yb-doped phosphate glass sample.
The plot shows the laser output power of the 9.5-mm-long WGL as a function of pump power. The inset shows the blue cooperative luminescence along the device whilst pumping at 976 nm.

5 WBG applications

5.1 WGLs

Femtosecond laser-written WBGs as with FBGs can be made into WGLs when fabricated into doped materials. WBGs can be used either as distributed Bragg reflectors (DBRs), akin to mirrors in a conventional laser cavity, or as a single feedback gain element, as in the case of DFB lasers. The optimisation of WGLs is achieved by matching the grating strength to the useable waveguide length (which is determined by the absorption/emission characteristics of the material) and mode matching the pump mode and waveguide mode. In low gain cross-section materials, such as glass, minimising the PL is also particularly important.

Taccheo et al. obtained the first femtosecond laser-written WGL with 1.7 mW output power at 1533.5 nm using a FBG-waveguide-FBG arrangement [78]. True monolithic WGL operation was subsequently demonstrated by Marshall et al. in a DFB configuration [6, 30]. In this case, a 20-mm-long Er:Yb codoped phosphate glass with a 500 nm period WBG lased when pumped with 710 mW at 976 nm. The DFB laser operated at 1537.6 nm with approximately 1 mW output power.

Improved laser performance was obtained by Ams et al. in a higher gain Yb-doped phosphate glass [42]. In this case, 102 mW of output power at 1032.6 nm in a 9.5-mm-long sample was achieved (Figure 20). The WBG had a maximum n_{eff} of 1.4×10^{-3} and a grating contrast lower bound of $\Delta n_{\text{AC}}=1.1\times10^{-4}$. The birefringence of the WBGs was approximately 2×10^{-6} similar to that obtained by Fernandes et al. in fused silica [62].

Dual-wavelength laser operation (1025 and 1035 nm) was also obtained in a Yb-doped glass host by incorporating a periodically phase-modulated sampled WBG [75]. In such a scheme, phase shifts were inserted in the WBG every 300 periods and lasing was obtained only on the ±1 order resonances due to their enhanced feedback.

A feature that makes DFB lasers desirable light sources are their high spectral purity. To this end, a loss-compensated recirculating delayed self-heterodyne interferometer was used to measure the linewidth of a 9.7-mm-long DFB WGL in Yb-doped phosphate glass [79]. Duan et al. measured the linewidth to be 35 kHz at a delay of 306 μs, a result reported to be similar to that of a fibre DFB laser.

The phosphate glass host used in all the reports outlined above has the advantage of higher gain over the more common silicate host used in many fibre lasers. WGLs in phosphate hosts, however, degrade over time due to the annihilation of colour centres induced during WBG inscription. This results in a reduction of grating strength and, in terms of laser operation, reduced output power and a blue shift of the laser wavelength. Duan et al. however, demonstrated that DFB WGL operation could also be obtained in a lower emission cross-section silicate glass (Schott IOG-10) [68]. In this case, output powers of 15 mW were obtained from a nonoptimised configuration. In contrast to phosphate glass WGLs, the output power increased over time, which was attributed to a reduction in the PL.

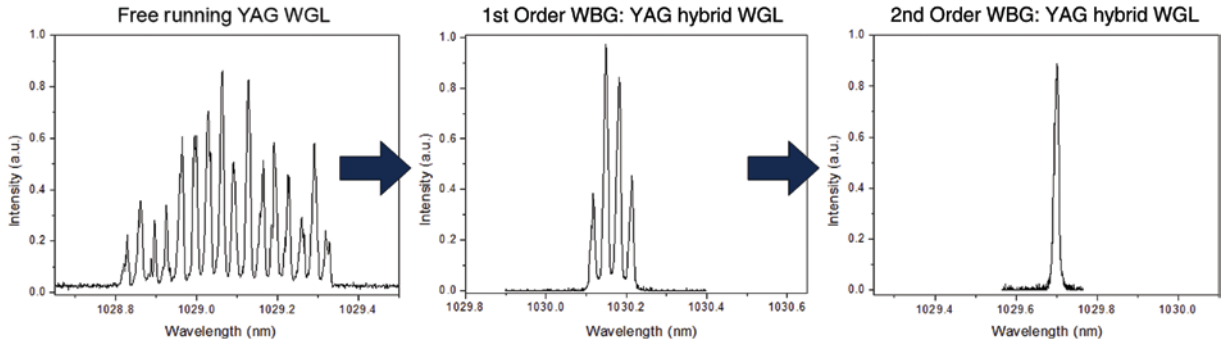


Figure 21: (Left) Broadband, multimode laser emission from a resonator formed between the Fresnel reflection of a Yb:YAG pump input facet and a thin high reflecting (HR) mirror at the other facet. Laser emission from the hybrid integration of an Yb:YAG WGL with (middle) a broad first-order WBG high reflector and (right) a narrow second-order WBG high reflector.

Rare-earth doped dielectric crystalline materials offer many advantages over glass hosts, for example, superior thermomechanical properties and higher peak emission/absorption cross-sections. Dekker et al. recently demonstrated laser operation using a hybrid WBG crystalline waveguide architecture [51]. In this case, a low loss, highly reflective WBG was coupled to a high gain, multilongitudinal line Yb : YAG WGL. Hybrid integration increased the spectral brightness by an order of magnitude, with the resultant laser operating on a single longitudinal mode (Figure 21).

Table 2 summarises the WGLs fabricated using ULI that use WBGs as a feedback element.

5.2 Sensors and filters

5.2.1 Sensor network

Gratings can be used as direct sensing elements calibrated to a shift in their reflection/transmission spectra. Properties that change the modal index or grating pitch of a grating will in turn shift the Bragg wavelength and thus can be monitored. Temperature, strain, and pressure are examples of various physical quantities that can be measured [14, 15].

The versatile sensing capabilities of WBGs were exemplified by Zhang et al. who used the ULI technique to fabricate a robust 3D optical sensor network in a thin sheet of fused silica glass [66]. The network consisted of a cascaded mesh of 12 multiplexed WBGs in a dual planar arrangement creating nine sensing zones. By placing gratings on both the top and the bottom of a 1-mm-thick, 50×50 mm sheet of glass, both tensile and compressive strain were measured using a calibrated coefficient of 1.23 pm/$\mu\varepsilon$. The device was also tested at high temperatures and found to remain viable up to 500°C with a thermal response of 10.4 pm/°C.

5.2.2 3D shape sensor

ULI is not restricted to a planar substrate. Lee et al. demonstrated a 3D laser-written shape, position, and temperature sensor in a coreless 125-µm-diameter optical fibre [80]. The sensor used a 1×3 directional coupler to distribute light into center and off-center fibre positions located at the vertices of an isosceles triangle arrangement

Table 2: Summary of the WGLs fabricated using ULI that use WBGs as a feedback element.

Substrate	Laser type	Laser wavelength λ_L (nm)	Output power (mW)	Notes
Er:Yb phosphate [6, 30]	DFB	1537.6	1	Near threshold
Yb phosphate [42]	DFB	1032.6	102	17.3% Slope efficiency
Yb phosphate [75]	DFB	985–1085	>10	100 nm gain bandwidth
Yb phosphate [75]	Sampled DFB	1025 and 1035	5 per channel	Dual wavelength
Yb phosphate [79]	DFB	1030	16	Linewidth 35.4 kHz
Yb phosphate [68]	DFB	1030	Decayed from 12	Colour centres anneal
Yb silicate [68]	DFB	1030	>12	Long lifetime (stable)
Yb YAG/borosilicate [51]	Hybrid DBR	1030	23	Single longitudinal mode

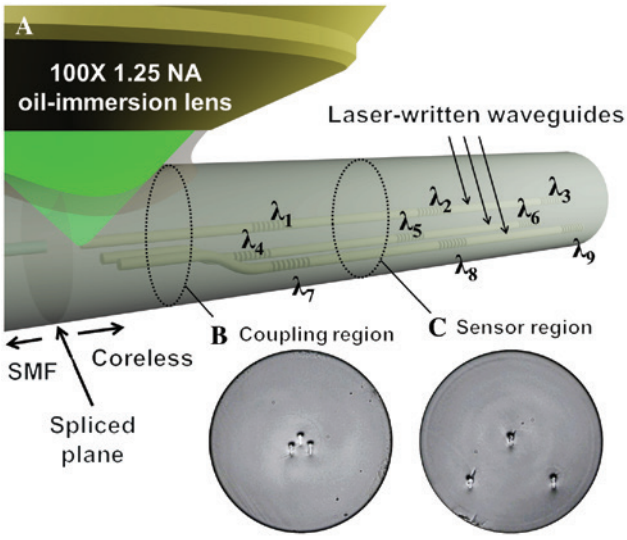


Figure 22: (A) Schematic of a 3D shape and thermal sensor written into coreless fused silica fibre by ULI. Microscope images of the fibre cross-section (125 μm diameter) at the (B) coupling and (C) sensor regions, showing the arrangement of the internal laser-written waveguides and WBGs. Reprinted with permission from [80].

(Figure 22). Each coupler arm consisted of three cascaded WBGs with 5 nm increments starting at 1280 nm. Interrogation was made possible through a fusion-spliced single-mode fibre at a 1 kHz sampling frequency. The geometry of nine axially and radially distributed WBG sensors allowed for simultaneous temperature and strain measurements to be made, from which real-time shape and thermal profiles were calculated. The fibre sensor was calibrated for bend sensing up to 0.025 mm^{-1} curvature and temperatures up to 250°C.

5.2.3 Edge filter

Edge filters or long-pass filters are standard bulk optical components used for spectral shaping, filtering, and sensing. Using the modulated burst method and a 1.25 NA oil immersion objective, Grenier et al. were able to fabricate edge filters in bulk fused silica with an attenuation of OD4 over 30 nm and OD2 over 300 nm [46].

The edge filters were realised by creating WBGs with small asymmetric cross-sections and large effective MFDs. This facilitated strong coupling to the continuum of radiation modes on the short wavelength side and a very sharp cut-on of 185 dB/nm to the Bragg resonance, resulting in a strongly isolating (43 dB) optical edge filter. The device had an IL of 7 dB mostly due to the high PL of the asymmetric WBGs; however, trade-offs between reduced loses and reduced extinction ratios are possible.

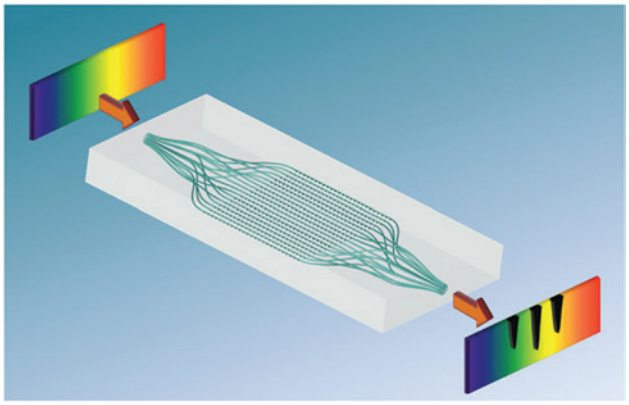


Figure 23: Narrowband spectral filtering of multimode light on a 3D integrated chip using photonic lanterns and WBGs.
The device was fabricated in a boro-aluminosilicate (Eagle2000) sample using ULI. Reprinted with permission from [50].

5.2.4 Multimode photonic lantern filter

A photonic lantern is an adiabatically tapered transition from a multimode waveguide to a number of single-mode waveguides [81]. Photonic lanterns find application in astrophotonics and telecommunications and, because of their inherent 3D nature, are well suited for fabrication using ULI. Thomson et al. were the first to demonstrate a laser-written photonic lantern [82] and Spaleniak et al. reported the first narrowband spectral filter of multimode light using photonic lanterns integrated with WBGs [50].

The integrated device consisted of back-to-back photonic lanterns with 19 single-mode waveguides in between (Figure 23). In each of these waveguides, up to four WBGs were written spatially across the same core using the PbP method. Coupling coefficients of 120 m^{-1} were achieved with a stop-band FWHM of 100 pm.

5.3 Exotic materials

5.3.1 Lithium niobate

The birefringence of WBGs written into crystalline media, with large electro-optic coefficients, can be dynamically controlled. This was demonstrated by Horn et al. [45] and subsequently Kroesen et al. [49] in lithium niobate.

Horn et al. wrote modulated parallel damage tracks in X-cut lithium niobate to create single-mode WBGs near 1550 nm. Grating reflectivities of 6% were achieved, although up to 18% was possible with increased side

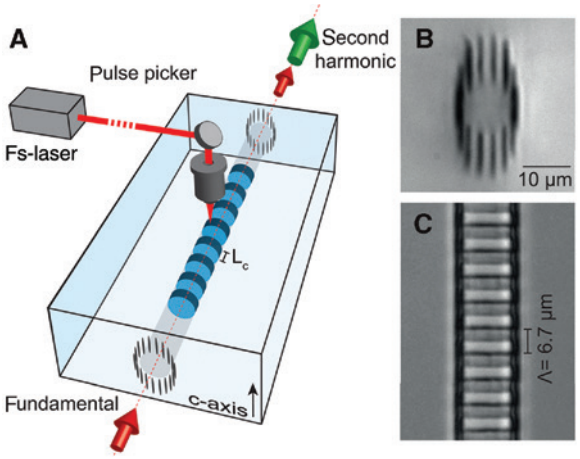


Figure 24: (A) Schematic of a QPM waveguide in z-cut lithium niobate. Optical microscope images of the (B) circular waveguide structure and (C) top view of the multiscan WBG. Reprinted with permission from [83].

lobes. The electro-optic tuning of the WBG spectral response was achieved by writing 100 μm deep channels, filled with silver, 7 μm away from the WBG structure to form electrodes. By applying a static external electric field, a tunability of 625 pm was achieved.

Kroesen et al. demonstrated high bandwidth tunability in lithium niobate of more than a peak width. This was achieved by writing a type II circular depressed cladding waveguide with an internal 10 pass type I multiscan WBG. The WBG reflectivity was 8% and the PL for the ordinary and extraordinary polarisation was 1.1 to 1.6 and 3 to 3.8 dB/cm, respectively. A tuning range of ±0.6 nm for a ±840 V electric field was demonstrated at 1526 nm.

WBGs in lithium niobate may conserve the electro-optic coefficient as used above; however, the nonlinear coefficients are not conserved. Recently, Kroesen et al. demonstrated quasi-phase-matched (QPM) waveguides using the modulation of the $\chi^{(2)}$ nonlinearity within the coherence length rather than typical domain inversion of periodically poled lithium niobate [83]. By writing a depressed cladding waveguide and an internal 6.7 μm pitch multiscan grating (Figure 24), the authors were able to demonstrate 5% second harmonic conversion from 1064 to 532 nm.

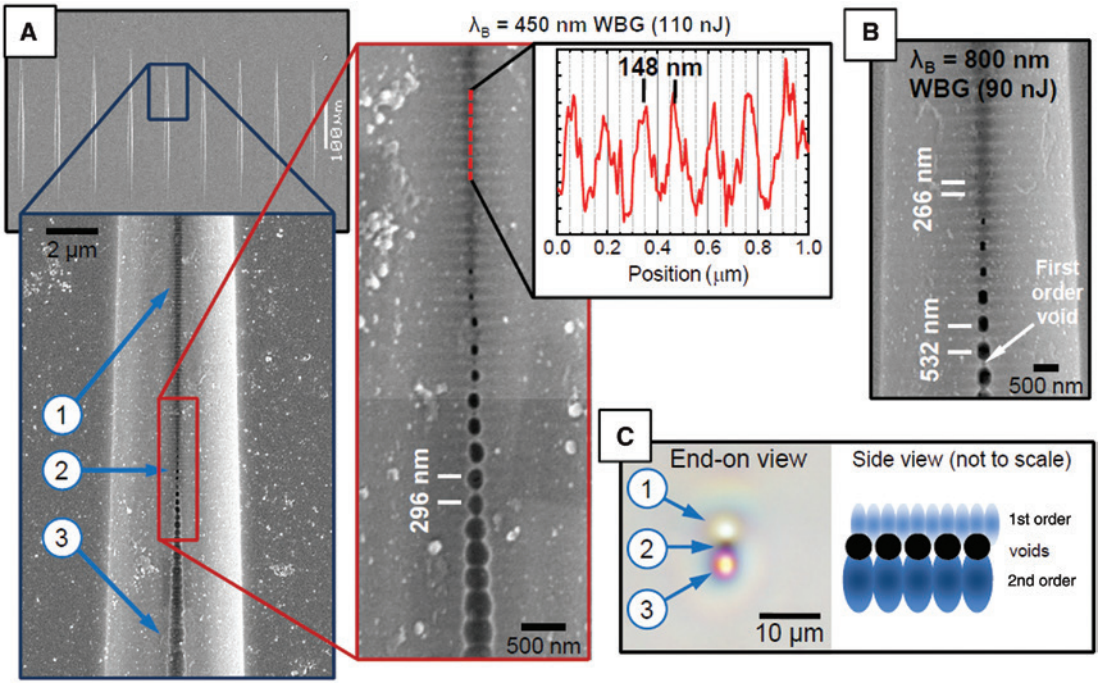


Figure 25: (A) Scanning electron microscopy (SEM) images of WBGs with periods of 148 nm. The top left image shows an overview of a WBG set looking straight onto an angled polished face of the sample. In all images, the writing laser was incident from the top. A profile along the vertical dashed red line is shown in the top right corner. (B) Each WBG, irrespective of its Bragg wavelength, showed a first-order structure above the focal spot and second-order structure below the focal spot with microvoids in between (λ_B = 800 nm illustrated for clarity). The white arrow marks a tiny first-order damage. (C) Three regions are apparent in the end-on view, which can be correlated with the SEM images. Above the focal spot (1) is a first-order grating structure, at the focal spot (2) are second-order periodic voids, and below (3) are second-order grating modifications.

5.3.2 Chalcogenide

Gratings operating in the mid-infrared region are of great interest in astrophotonics. Chalcogenides being transparent up to 5 μm are a potential host for this application. Through spatial and temporal beam shaping, McMillen et al. reported WBGs with circular cross-sections in GLS chalcogenide glass [48]. The strongest WBGs were written with a 25% duty cycle, were single mode at 1550 nm, and had grating depths of up to 25 dB.

5.4 Visible WBGs

Short-wavelength WBGs written using the ULI technique would in theory be limited by the size of the focal spot of the writing laser and the closely spaced grating pitch. However, due to the nonlinear nature of femtosecond laser pulse absorption by the material, internal focal volumes less than 25% of the writing wavelength can be achieved.

Using a 1.0 NA objective and a laser repetition rate of 55 kHz, Gross et al. inscribed single-scan, first-order PbP WBGs in a boro-aluminosilicate (Eagle2000) sample with pitches ranging from 270 nm ($\lambda_B = 800$ nm) down to 148 nm ($\lambda_B = 450$ nm) [24, 41]. Each grating, irrespective of its Bragg wavelength, showed a first-order structure above the focal spot and second-order structure below with microvoids in between (as illustrated in Figure 25). Grating periods as close as 148 nm ($\lambda_B = 450$ nm) were resolved within the upper positive index change region. Due to the unavailability of relevant diagnostics, these WBGs were never characterised. The 650 to 800 nm WBGs were spectrally characterised in transmission. The 15-mm-long WBGs had transmission dips of 11.8 dB at 648 nm ($\kappa = 136$ m^{-1}), 17.8 dB at 698 nm ($\kappa = 183$ m^{-1}), 18.4 dB at 748 nm ($\kappa = 187$ m^{-1}), and 15.3 dB at 798 nm ($\kappa = 163$ m^{-1}).

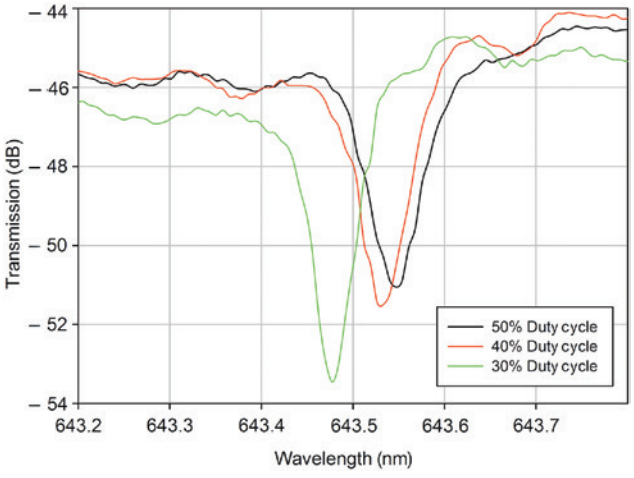


Figure 26: First-order WBGs fabricated in the visible spectrum using a 1 kHz laser and the modulated burst method.
A coupling coefficient of $\kappa = 314$ m^{-1} was measured in the alumino-borosilicate glass.

Figure 26 shows that first-order WBGs at visible wavelengths can also be realised using the modulated burst method. In this simpler case, a 1 kHz laser and a focussing objective with a 0.6 NA was used to create single-mode WBGs at 643 nm based purely on a type I positive index change. A number of duty cycles were tested in a borosilicate glass with the strongest WBG having a coupling coefficient of $\kappa = 314$ m^{-1}. Tighter focussing objectives could be used to fabricate WBGs at shorter wavelengths.

5.5 Optofluidics

Lab-on-Chip (LOC) detection systems can be used as a remote point-of-care solution by replacing larger, high-cost, bench-top instrumentation. LOCs can be used for the measurement of fluorescence or absorption of analytes and for cytometry more generally. ULI is well placed as a tool in this area due to the ability to fabricate waveguides, Bragg gratings, and microfluidic channels in 3D [84].

Maselli et al. fabricated an optofluidic sensor by integrating a WBG and a microfluidic channel in a fused silica sample [85]. The microfluidic channel was obtained by postprocessing a large waveguide structure in dilute hydrofluoric acid for 2.5 h. The evanescent field penetration of the WBG mode into the closely positioned microfluidic channel induced a Bragg wavelength shift, which was dependent on the refractive index of the fluid in the channel. By also incorporating reference WBGs in the chip, temperature and strain were compensated for allowing accurate measurements of fluidic refractive indices ranging from 1 to 1.452. The optofluidic sensor had a maximum sensitivity of 81 nm/riu or minimum detectable index change of 1.2×10^{-4}.

6 Conclusions

In this review, we have summarised the field of ultrafast laser-written WBGs since its first demonstration a decade ago. We show that WBGs can be fabricated in transparent bulk materials using numerous methodologies with each pathway specific to the host and set of writing parameters. The careful control of the chosen fabrication technique enables the WBG characteristics to

be tailored to suit particular target applications of which WBGs have many. With integrated photonics playing an ever increasing role in new technologies, WBGs look to have a secured future.

Acknowledgments: This research was conducted with the Australian Research Council Centre of Excellence for Ultrahigh Bandwidth Devices for Optical Systems (project number CE110001018) and the assistance of the LIEF programs. This work was performed in part at the OptoFab node of the Australian National Fabrication Facility, using NCRIS and state government funding.

References

[1] Davis KM, Miura K, Sugimoto N, Hirao K. Writing waveguides in glass with a femtosecond laser. Opt Lett 1996;21:1729–31.
[2] Glezer EN, Milosavljevic M, Huang L, et al. Three-dimensional optical storage inside transparent materials. Opt Lett 1996;21:2023–5.
[3] Gross S, Dubov M, Withford MJ. On the use of the type I and II scheme for classifying ultrafast laser direct-write photonics. Opt Express 2015;23:7767.
[4] Gattass RR, Mazur E. Femtosecond laser micromachining in transparent materials. Nat Photon 2008;2:219–25.
[5] Della Valle G, Osellame R, Laporta P. Micromachining of photonic devices by femtosecond laser pulses. J Opt A Pure Appl Opt 2009;11:13001.
[6] Ams M, Marshall GD, Dekker P, Piper JA, Withford MJ. Ultrafast laser written active devices. Laser Photon Rev 2009;3:535–44.
[7] Ams M, Little DJ, Withford MJ. Femtosecond-laser-induced refractive index modifications for photonic device processing. In: Laser Growth and Processing of Photonic Devices, Vainos NA, ed. Chapter 10. Cambridge, UK, Woodhead Publishing Limited, 2012:305–32.
[8] Osellame R, Cerullo G, Ramponi R, eds. Femtosecond Laser Micromachining, Volume 123 of Topics in Applied Physics. Berlin/Heidelberg, Springer, 2012.
[9] Choudhury D, Macdonald JR, Kar AK. Ultrafast laser inscription: perspectives on future integrated applications. Laser Photon Rev 2014;8:827–46.
[10] Gross S, Withford MJ. Ultrafast-laser-inscribed 3D integrated photonics: challenges and emerging applications, Nanophotonics 2015;4:332–52.
[11] Stoian R, D'Amico C, Bhuyan M, Cheng G. Ultrafast laser photoinscription of large-mode-area waveguiding structures in bulk dielectrics. Opt Laser Technol 2016;80:98–103.
[12] Marshall GD, Ams M, Withford MJ. Direct laser written waveguide-Bragg gratings in bulk fused silica. Opt Lett 2006;31:2690–1.
[13] Hill K, Meltz G. Fiber Bragg grating technology fundamentals and overview. J Lightw Technol 1997;15:1263–76.
[14] Kashyap R. Fiber Bragg Gratings Academic Press. 2nd ed. Burlington, MA, USA, Elsevier, 2009.
[15] Othonos A, Kalli K. Fiber Bragg gratings: fundamentals and applications in telecommunications and sensing. Norwood, MA, Artech House, Inc., 1999.
[16] Thomas JU, Voigtländer C, Becker RG, Richter D, Tünnermann A, Nolte S. Femtosecond pulse written fiber gratings: a new avenue to integrated fiber technology. Laser Photon Rev 2012;6:709–23.
[17] Malo B, Hill K, Bilodeau F, Johnson DC, Albert J. Point-by-point fabrication of micro-Bragg gratings in photosensitive fiber using single excimer pulse refractive-index modification techniques. Electron Lett 1993;29:1668–9.
[18] Martinez A, Dubov M, Khrushchev I, Bennion I. Direct writing of fibre Bragg gratings by femtosecond laser. Electron Lett 2004;40:1170–2.
[19] Wikszak E, Burghoff J, Will M, Nolte S, Tünnermann A, Gabler T. Recording of fiber Bragg gratings with femtosecond pulses using a "point by point" technique. In: Conference on Lasers and Electro-Optics (CLEO), Burghoff J, ed., Vol 2, CThM7, 2004.
[20] Kamata M, Obara M. Waveguide-based Bragg filters inside bulk glasses integrated by femtosecond laser processing. In: CLEO/Europe, 2005 Conference on Lasers and Electro-Optics Europe. IEEE, 2005.
[21] Zhang HB, Eaton SM, Li JZ, Herman PR. Type II femtosecond laser writing of Bragg grating waveguides in bulk glass. Electron Lett 2006;42:1223–4.
[22] Zhang HB, Eaton SM, Li JZ, Herman PR. Femtosecond laser direct writing of multiwavelength Bragg grating waveguides in glass. Opt Lett 2006;31:3495–7.
[23] Zhang HB, Eaton SM, Li JZ, Nejadmalayeri AH, Herman PR. Type II high-strength Bragg grating waveguides photowritten with ultrashort laser pulses. Opt Express 2007;15:4182–91.
[24] Gross S, Withford MJ, Fuerbach A. Direct laser inscription of 270 nm period waveguide Bragg gratings. In: Conference on Lasers and Electro-Optics. Pacific Rim Optical Society of America, 2011:C848.
[25] Thiel M, Flachenecker G, Schade W. Femtosecond laser writing of Bragg grating waveguide bundles in bulk glass. Opt Lett 2015;40:1266.
[26] Zhang HB, Eaton SM, Herman PR. Single-step writing of Bragg grating waveguides in fused silica with an externally modulated femtosecond fiber laser. Opt Lett 2007;32:2559–61.
[27] Chung JH, Gu Y, Fujimoto JG. Submicron-period waveguide Bragg gratings direct written by an 800-nm femtosecond oscillator. In: Conference on Lasers and Electro-Optics. Optical Society of America, 2007:CThS4.
[28] Miese CT, Withford MJ, Fuerbach A. Femtosecond laser direct-writing of waveguide Bragg gratings in a quasi cumulative heating regime. Opt Express 2011;19:19542.
[29] Gross S, Ams M, Lancaster DG, Monro TM, Fuerbach A, Withford MJ. Femtosecond direct-write überstructure waveguide Bragg gratings in ZBLAN. Opt Lett 2012;37:3999.
[30] Marshall GD, Dekker P, Ams M, Piper JA, Withford MJ. Directly written monolithic waveguide laser incorporating a distributed feedback waveguide-Bragg grating. Opt Lett 2008;33:956–8.
[31] Ha S, Ams M, Marshall GD, et al. Control of light transmission in laser-written phase-shifted Bragg grating couplers. Opt Lett 2011;36:1380–2.
[32] Marshall GD, Jesacher A, Thayil A, Withford MJ, Booth MJ. Three-dimensional imaging of direct-written photonic structures. Opt Lett 2011;36:695.
[33] Ams M, Marshall GD, Spence DJ, Withford MJ. Slit beam shaping method for femtosecond laser direct-write fabrication of symmetric waveguides in bulk glasses. Opt Express 2005;13:5676–81.

[34] Yariv A. Coupled-mode theory for guided-wave optics. IEEE J Quantum Electron 1973;9:919–33.
[35] Bass M, Enoch JM, Van Stryland EW, Wolfe WL. Handbook of Optics. Volume IV. 2nd ed. New York, McGraw-Hill Professional, 1995.
[36] Erdogan T. Fiber grating spectra. J Lightw Technol 1997;15:1277–94.
[37] Bragg WL. The diffraction of short electromagnetic waves by a crystal. Proc Cambr Philos Soc 1914;17:43–57.
[38] Kogelnik H. Coupled wave theory for thick hologram gratings. Bell Syst Tech J 1969;48:2909–47.
[39] Mizrahi V, Sipe JE. Optical properties of photosensitive fiber phase gratings. J Lightw Technol 1993;11:1513–7.
[40] Sipe JE, Poladian L, de Sterke CM. Propagation through nonuniform grating structures. J Opt Soc Am A 1994;11:1307.
[41] Gross S. Direct-write mid-IR waveguide lasers. Ph.D thesis, Macquarie University, 2012.
[42] Ams M, Dekker P, Marshall GD, Withford MJ. Monolithic 100 mW Yb waveguide laser fabricated using the femtosecond-laser direct-write technique. Opt Lett 2009;34:247–9.
[43] Dolgaleva K, Malacarne A, Tannouri P, et al. Integrated optical temporal Fourier transformer based on a chirped Bragg grating waveguide. Opt Lett 2011;36:4416–8.
[44] Brown G, Thomson RR, Kar AK, Psaila ND, Bookey HT. Ultrafast laser inscription of Bragg-grating waveguides using the multiscan technique. Opt Lett 2012;37:491.
[45] Horn W, Kroesen S, Herrmann J, Imbrock J, Denz C. Electro-optical tunable waveguide Bragg gratings in lithium niobate induced by femtosecond laser writing. Opt Express 2012;20:26922.
[46] Grenier JR, Fernandes LA, Herman PR. Femtosecond laser writing of optical edge filters in fused silica optical waveguides. Opt Express 2013;21:4493.
[47] Zeil P, Voigtländer C, Thomas JU, Richter D, Nolte S. Femtosecond laser-induced apodized Bragg grating waveguides. Opt Lett 2013;38:2354.
[48] McMillen BW, Li M, Huang S, Zhang B, Chen KP. Ultrafast laser fabrication of Bragg waveguides in chalcogenide glass. Opt Lett 2014;39:3579–82.
[49] Kroesen S, Horn W, Imbrock J, Denz C. Electro-optical tunable waveguide embedded multiscan Bragg gratings in lithium niobate by direct femtosecond laser writing. Opt Express 2014;22:23339.
[50] Spaleniak I, Gross S, Jovanovic N, et al. Multiband processing of multimode light: combining 3D photonic lanterns with waveguide Bragg gratings. Laser Photon Rev 2014;8:L1–5.
[51] Dekker P, Ams M, Calmano T, et al. Spectral narrowing of Yb:YAG waveguide lasers through hybrid integration with ultrafast laser written Bragg gratings. Opt Express 2015;23:20195.
[52] Babic D, Corzine S. Analytic expressions for the reflection delay, penetration depth, and absorptance of quarter-wave dielectric mirrors. IEEE J Quantum Electron 1992;28:514–24.
[53] Yelen K, Hickey LMB, Zervas MN. A new design approach for fiber DFB lasers with improved efficiency. IEEE J Quantum Electron 2004;40:711–20.
[54] Little DJ, Ams M, Dekker P, Marshall GD, Dawes JM, Withford MJ. Femtosecond laser modification of fused silica: the effect of writing polarization on Si-O ring structure. Opt Express 2008;16:20029–37.
[55] Gross S, Ams M, Palmer G, et al. Ultrafast laser inscription in soft glasses: a comparative study of athermal and thermal processing regimes for guided wave optics. Int J Appl Glass Sci 2012;3:332–48.
[56] Schaffer CB, Garcia JF, Mazur E. Bulk heating of transparent materials using a high-repetition-rate femtosecond laser. Appl Phys A Mater Sci Process 2003;76:351–4.
[57] Eaton SM, Zhang HB, Herman PR, et al. Heat accumulation effects in femtosecond laser-written waveguides with variable repetition rate. Opt Express 2005;13:4708–16.
[58] Jovanovic N, Gross S, Miese C, Fuerbach A, Lawrence J, Withford MJ. Direct laser written multimode waveguides for astronomical applications. In: Proc. SPIE 7739, Modern Technologies in Space- and Ground-Based Telescopes and Instrumentation. International Society for Optics and Photonics, San Diego, CA, 2010:773923.
[59] Arriola A, Gross S, Jovanovic N, et al. Low bend loss waveguides enable compact, efficient 3D photonic chips. Opt Express 2013;21:2978.
[60] Marcuse D. Light Transmission Optics. 1st ed. New York, Van Nostrand Reinhold Company, 1972.
[61] Tittelbach G, Richter B, Karthe W. Comparison of three transmission methods for integrated optical waveguide propagation loss measurement. Pure Appl Opt J Eur Opt Soc Pt A 1993;2:683–700.
[62] Fernandes LA, Grenier JR, Herman PR, Aitchison JS, Marques PVS. Stress induced birefringence tuning in femtosecond laser fabricated waveguides in fused silica. Opt Express 2012;20:24103.
[63] Sudrie L, Franco M, Prade B, Mysyrewicz A, Mysyrowicz A. Writing of permanent birefringent microlayers in bulk fused silica with femtosecond laser pulses. Opt Commun 1999;171:279–84.
[64] Shimotsuma Y, Kazansky PG, Qiu JR, Hirao K. Self-organized nanogratings in glass irradiated by ultrashort light pulses. Phys Rev Lett 2003;91:247405.
[65] Fernandes LA, Grenier JR, Herman PR, Aitchison JS, Marques PVS. Femtosecond laser fabrication of birefringent directional couplers as polarization beam splitters in fused silica. Opt Express 2011;19:11992–9.
[66] Zhang HB, Ho S, Eaton SM, Li JZ, Herman PR. Three-dimensional optical sensing network written in fused silica glass with femtosecond laser. Opt Express 2008;16:14015–23.
[67] Dekker P, Ams M, Marshall GD, Little DJ, Withford MJ. Annealing dynamics of waveguide Bragg gratings: evidence of femtosecond laser induced colour centres. Opt Express 2010;18:3274–83.
[68] Duan Y, Dekker P, Ams M, Palmer G, Withford MJ. Time dependent study of femtosecond laser written waveguide lasers in Yb-doped silicate and phosphate glass. Opt Mater Express 2015;5:416.
[69] Malo B, Hill K, Thériault S, Bilodeau F, Johnson D, Albert J. Apodised in-fibre Bragg grating reflectors photoimprinted using a phase mask. Electron Lett 1995;31:223–5.
[70] Voigtländer C, Zeil P, Thomas JU, et al. Fs laser induced apodised Bragg waveguides in fused silica. Proc SPIE 2011;7925:79250Y–79250Y-7.
[71] Williams RJ, Voigtländer C, Marshall GD, et al. Point-by-point inscription of apodized fiber Bragg gratings. Opt Lett 2011;36:2988.
[72] Zhang HB, Herman PR. Femtosecond laser direct writing of chirped Bragg grating waveguides inside fused silica glass. In: Bragg Gratings, Photosensitivity, and Poling in Glass Waveguides. Washington, DC, OSA, 2007.

[73] Zhang HB, Herman PR. Chirped Bragg grating waveguides directly written inside fused silica glass with an externally modulated ultrashort fiber laser. Photon Technol Lett IEEE 2009;21:277–9.
[74] Haus H, Shank C. Antisymmetric taper of distributed feedback lasers. IEEE J Quantum Electron 1976;12:532–9.
[75] Ams M, Dekker P, Marshall GD, Withford MJ. Ultrafast laser-written dual-wavelength waveguide laser. Opt Lett 2012;37:993–5.
[76] Grenier JR, Fernandes LA, Aitchison JS, Marques PVS, Herman PR. Femtosecond laser fabrication of phase-shifted Bragg grating waveguides in fused silica. Opt Lett 2012;37:2289.
[77] Eggleton BJ, Krug PA, Poladian L, Ouellette F. Long periodic superstructure Bragg gratings in optical fibres. Electron Lett 1994;30:1620–2.
[78] Taccheo S, Della Valle G, Osellame R, et al. Er:Yb-doped waveguide laser fabricated by femtosecond laser pulses. Opt Lett 2004;29:2626–8.
[79] Duan Y, Dekker P, Jaatinen E, et al. Narrow linewidth DFB waveguide laser fabricated via ultrafast laser inscription. IEEE Photon Technol Lett 2014;26:2499–502.
[80] Lee KKC, Mariampillai A, Haque M, Standish BA, Yang VXD, Herman PR. Temperature-compensated fiber-optic 3D shape sensor based on femtosecond laser direct-written Bragg grating waveguides. Opt Express 2013;21:24076–86.
[81] Birks TA, Gris-Sánchez I, Yerolatsitis S, Leon-Saval SG, Thomson RR. The photonic lantern. Adv Opt Photon 2015;7:107.
[82] Thomson RR, Birks TA, Leon-Saval SG, Kar AK, Bland-HawtHorn J. Ultrafast laser inscription of an integrated photonic lantern. Opt Express 2011;19:5698–705.
[83] Kroesen S, Tekce K, Imbrock J, Denz C. Monolithic fabrication of quasi phase-matched waveguides by femtosecond laser structuring the $\chi(2)$ nonlinearity. Appl Phys Lett 2015;107:101109.
[84] Osellame R, Hoekstra HJWM, Cerullo G, Pollnau M. Femtosecond laser microstructuring: an enabling tool for optofluidic Lab-on-Chips. Laser Photon Rev 2011;5:442–63.
[85] Maselli V, Grenier JR, Ho S, Herman PR. Femtosecond laser written optofluidic sensor: Bragg grating waveguide evanescent probing of microfluidic channel. Opt Express 2009;17:11719–29.